1	Gene activation precedes DNA demethylation in response to infection in human dendritic cells
2	
3	Alain Pacis ^{1,2‡} , Florence Mailhot-Léonard ^{1,2‡} , Ludovic Tailleux ^{3,4} , Haley E Randolph ^{1,2} , Vania Yotova ¹ ,
4	Anne Dumaine ¹ , Jean-Christophe Grenier ¹ , Luis B Barreiro ^{1,5,6*,}
5	
6	¹ CHU Sainte-Justine Research Center, Department of Genetics, Montreal, H3T1C5, Canada; ² University
7	of Montreal, Department of Biochemistry, Montreal, H3T1J4, Canada; ³ Institut Pasteur, Mycobacterial
8	Genetics Unit, Paris, 75015, France; ⁴ Institut Pasteur, Unit for Integrated Mycobacterial Pathogenomics,
9	CNRS UMR 3525, Paris, 75015, France; ⁵ University of Montreal, Department of Pediatrics, Montreal,
10	H3T1J4, Canada; ⁶ University of Chicago, Department of Medicine, Genetics Section, Chicago, Illinois,
11	USA.
12	
13	
14	‡ These authors equally contributed to this study.
15	*Correspondence to: lbarreiro@uchicago.edu
16	Running title: Epigenetic changes in response to infection
17	Keywords: DNA Methylation, Infection, Enhancers, Gene regulation
18	

19 ABSTRACT

DNA methylation is considered to be a relatively stable epigenetic mark. Yet, a growing body of evidence 20 21 indicates that DNA methylation levels can change rapidly, for example, in innate immune cells facing an 22 infectious agent. Nevertheless, the causal relationship between changes in DNA methylation and gene 23 expression during infection remains to be elucidated. Here, we generated time-course data on DNA 24 methylation, gene expression, and chromatin accessibility patterns during infection of human dendritic 25 cells with Mycobacterium tuberculosis. We found that the immune response to infection is accompanied 26 by active demethylation of thousands of CpG sites overlapping distal enhancer elements. However, 27 virtually all changes in gene expression in response to infection occur prior to detectable changes in DNA 28 methylation, indicating that the observed losses in methylation are a downstream consequence of 29 transcriptional activation. Footprinting analysis revealed that immune-related transcription factors (TF), 30 such as NF- κ B/Rel, are recruited to enhancer elements prior to the observed losses in methylation, 31 suggesting that DNA demethylation is mediated by TF binding to cis-acting elements. Collectively, our 32 results show that DNA demethylation is not required for the establishment of the core regulatory program 33 engaged upon infection. 34

- 35
- 36
- 37
- 38
- 39
- 40
- 41

42 INTRODUCTION

43 Innate immune cells, such as dendritic cells (DCs) and macrophages, are the first mediators recruited in response to an invading pathogen. Upon stimulation, these cells considerably shift their transcriptional 44 45 program, activating hundreds of genes involved in immune-related processes in a rapid and highly 46 choreographed fashion. This is achieved through the binding of signal-dependent transcription factors 47 (TFs), including NF- κ B/Rel, AP-1, and interferon regulatory factors (IRFs), to gene regulatory regions of 48 the genome where recruitment of various co-activators is initiated [1, 2]. Alterations to the epigenome, 49 such as histone modifications and DNA methylation, are recognized as important permissive or 50 suppressive factors that play an integral role in modulating access of TFs to cis-acting DNA regulatory 51 elements via the regulation of chromatin dynamics. Consequently, changes to the epigenetic landscape are 52 expected to have a significant impact on gene expression.

53

54 Many studies have highlighted the importance of histone modifications in regulating complex gene 55 expression programs underlying immune responses [3, 4]. However, the exact role that DNA methylation 56 plays in innate immune response regulation remains ambiguous. We have previously shown that infection 57 of post-mitotic DCs is associated with an active loss of methylation at enhancers and that such 58 demethylation events are strongly predictive of changes in expression levels of nearby genes [5]. Many 59 other studies correlate these two processes [6-13], but it remains unclear whether altered methylation 60 patterns directly invoke transcriptional modulation or whether such patterns are the downstream 61 consequence of TF binding to regulatory regions. Thus, the causal relationship between changes in DNA 62 methylation and gene expression during infection remains unresolved. To address this question, we 63 characterized in parallel genome-wide patterns of DNA methylation, gene expression, and chromatin 64 accessibility in non-infected and Mycobacterium tuberculosis (MTB)-infected DCs at multiple time 65 points. Our results show that the loss of DNA methylation observed in response to infection is not required for the activation of most enhancer elements and that, instead, demethylation is a downstreamconsequence of TF binding.

68

69 **RESULTS**

70 Bacterial infection induces stable DNA demethylation at enhancers of dendritic cells

71 To investigate the relationship between changes in gene expression and DNA methylation in response to 72 infection, we infected monocyte-derived DCs from 4 healthy individuals with a live virulent strain of 73 Mycobacterium tuberculosis (MTB) for 2-, 18-, 48-, and 72-hours. At each time-point, we obtained single 74 base-pair resolution DNA methylation levels for over 130,000 CpG sites using a customized capturebased bisulfite sequencing panel (SeqCap Epi, see Methods), in matched non-infected 75 and MTB-76 infected DCs. Our customized SeqCap Epi panel interrogates 33,059 regions highly enriched among 77 putative enhancer elements (58% are associated with the H3K4me1 enhancer mark [14]; **Supplementary** 78 Figure 1A), which are the main targets of methylation changes in response to infection [5]. In total, we 79 generated ~717 million single-end reads (mean = 17.5 million reads per sample; Supplementary Table 80 1), resulting in an average coverage of $\sim 70 \text{X}$ per CpG site (Supplementary Figure 1B). Methylation 81 values between samples were strongly correlated, attesting to the high quality of the data 82 (Supplementary Figure 1C; median r across all samples = 0.94).

83

We next assessed temporal changes in methylation levels in response to infection using the DSS software [15]. We defined differentially methylated (DM) CpG sites as those showing a significant difference of methylation between infected and non-infected samples at a False Discovery Rate (FDR) < 0.01 and an absolute mean methylation difference above 10%. Using these criteria, we identified 6,174 DM CpG sites across the time course of infection. Consistent with previous findings [5], the vast majority of changes in methylation (87%) were associated with the loss of DNA methylation in infected cells (**Figure 1A,B**).

91 To test if live bacteria were required to induce the observed changes in DNA methylation, we collected 92 similar data on DCs exposed to heat-killed MTB in addition to the live MTB experiments. Changes in 93 methylation in response to live and heat-killed MTB were strikingly correlated, particularly at later time-94 points post-infection ($r \ge 0.84$ at 18h and above; Supplementary Figure 2). These results show that DCs 95 do not require exposure to a live pathogen to elicit the overall demethylation detected in response to 96 infection. Simply, the engagement of innate immune receptors and activation of pathways involved in 97 pathogen sensing and elimination is sufficient to induce methylation shifts. Hierarchical clustering 98 analysis of the DM sites observed when considering samples exposed to either live or heat-killed bacteria 99 showed that >80% of the sites exhibited a gradual loss of methylation over the time course of infection 100 until methylation marks were almost completely erased and that very few changes were detectable at 2 101 hours post-infection (DM Cluster 3; Figure 1C,D; Supplementary Table 2).

102

103 Monocyte-derived DCs do not proliferate in response to infection [5] and, therefore, any observed losses 104 in methylation must occur through an active mechanism involving the ten-eleven translocation (Tet) 105 enzymes, a family of enzymes that converts 5-methylcytosine (5mC) to 5-hydroxymethylcytosine (5hmC) 106 [16]. Thus, we used Tet-assisted bisulfite sequencing (TAB-seq) data collected from non-infected DCs [5] 107 to assess if DM sites had significantly different levels of 5hmC as compared to non-DM sites. We found 108 that DM sites (Cluster 3) show high levels of 5hmC even prior to infection (Figure 1E; 3.2-fold enrichment compared to non-DM sites; Wilcoxon test; $P < 1 \times 10^{-16}$), suggesting that DM sites are likely 109 pre-bound by TET enzymes (likely TET2 [17, 18], the most expressed Tet enzyme in DCs 110 111 (Supplementary Figure 3)) and that 5hmC may serve as a stable mark that acts to prime enhancers [19-112 21].

113

114 Up-regulation of inflammatory genes precedes DNA demethylation

We collected RNA-seq data from matched non-infected and infected samples at each time point, for a 115 total of 34 RNA-seq profiles across time-treatment combinations (mean = 42.2 million reads per sample; 116 117 Supplementary Table 1). The first principal component of the resulting gene expression data accounted 118 for 63% of the variance in our dataset and separated infected and non-infected DCs (Supplementary 119 Figure 4A). We found extensive differences in gene expression levels between infected and non-infected DCs: of the 13.956 genes analyzed, 1.987 (14%), 4.371 (31%), 4.591 (33%), and 5.189 (37%) were 120 121 differentially expressed (DE) at 2, 18, 48, and 72 hours post-infection, respectively (FDR < 0.01 and 122 absolute log2(fold change) > 1; Supplementary Table 3). We also collected RNA-seq data in samples 123 stimulated with heat-inactivated MTB and found that, similar to changes in methylation, changes in gene 124 expression in response to live and heat-inactivated MTB were strongly correlated (r ≥ 0.94 ; Supplementary Figure 4B). We next grouped the set of DE genes across the time course (7,457 in total) 125 126 into 6 distinct temporal expression clusters (Figure 2A,B; Supplementary Table 3). These clusters cover 127 a variety of differential expression patterns, including genes which show increasing up-regulation over 128 time (DE Cluster 5: Persistent induced; n = 2,091) to genes in which the highest levels of expression 129 occur at 2 or 18 hours followed by a decrease towards basal levels (DE Cluster 4: Early induced (n =130 765), and DE Cluster 6: Intermediate induced (n = 839), respectively) (Figure 2B). Gene ontology (GO) 131 enrichment analysis revealed that induced genes were strongly enriched among GO terms directly related to immune function, including defense response (FDR = 1.2×10^{-11}) and response to cytokine (FDR = 8.2 132 \times 10⁻¹²), whereas repressed genes were primarily enriched for gene sets associated with metabolic 133 134 processes (Figure 2C; Supplementary Table 4).

135

We next tested whether genes located near DM sites—particularly focusing on those sites exhibiting a stable loss of methylation (*i.e.*, Cluster 3 in Figure 1C,D)—were more likely to be differentially expressed upon MTB infection relative to all genes in the genome. We found that genes associated with one or more DM sites were strongly enriched among genes that were up-regulated in response to infection, regardless of the time point at which expression levels started to change: early (2.5-fold, $P = 3.23 \times 10^{-11}$), intermediate (3.5-fold, $P = 3.59 \times 10^{-25}$), and persistent (3.1-fold, $P = 3.80 \times 10^{-33}$) (Figure 2D,E).

142

143 If demethylation is required for the activation of enhancer elements and the subsequent up-regulation of 144 their target genes, we would expect demethylation to occur *prior* to changes in gene expression; instead, 145 we found the opposite pattern. Among up-regulated genes associated with DM sites (n = 593), 37% 146 exhibited at least a two-fold increase in gene expression levels at 2-hours post-infection, although 147 differential methylation did not begin to be detectable until 18-hours post-infection (Figure 2E). For only 148 17 genes (less than 3% of all up-regulated genes associated with DM sites), DNA demethylation occurred 149 prior to gene activation (Supplementary Figure 5), suggesting that no definitive causal relationship 150 between DNA demethylation and gene activation exists.

151

152 To confirm that our findings were generalizable to other innate immune cell types and pathogenic 153 infections, we performed a separate time-course analysis of differential methylation in Salmonella-154 infected macrophages from one additional donor over six time-points (Supplementary Table 1). We 155 discovered hundreds of CpG sites that exhibited a progressive loss of methylation over the time course of 156 infection, corroborating our findings in MTB-infected DCs (Figure 3A). To assess whether 157 demethylation arises after the activation of associated enhancers, we collected ChIP-seq data for 158 acetylation of histone 3 lysine 27 (H3K27ac) at 2-hours post-infection, as changes in DNA methylation 159 have yet to occur at this point. We found that the deposition of activating H3K27ac marks preceded 160 demethylation at these CpG sites (Figure 3B). Moreover, using previously published RNA-seq expression data from Salmonella-infected macrophages [22], we found that most genes associated with 161 162 these sites were up-regulated at 2-hours post-infection (Figure 3C), prior to any changes in methylation. 163 Collectively, these findings indicate that DNA demethylation is not required for the activation of most 164 enhancer elements and that the vast majority of methylation changes induced by infection are a165 downstream consequence of transcriptional activation.

166

167 The binding of most infection-induced TFs does not require active demethylation

168 We next asked whether MTB-induced gene expression changes were associated with changes in 169 chromatin accessibility. To do so, we profiled regions of open chromatin in non-infected and infected 170 DCs at the same time-points (plus one additional time-point at 24 hours) using ATAC-seq [23]. Overall, 171 we found that the response to MTB infection was accompanied by an increase in chromatin accessibility 172 across regulatory regions associated with genes up-regulated upon MTB infection, regardless of their 173 expression profiles (Figure 4A). Interestingly, most increases in chromatin accessibility were observed at 174 later stages of infection, suggesting that the activation of early response genes does not require significant 175 modifications to the chromatin structure.

176

177 To investigate the relationship between DNA methylation and TF occupancy, we performed TF footprinting analysis on our target regions (*i.e.*, the set of putative enhancers tested for dynamic DNA 178 179 methylation). We classified target regions as "hypomethylated regions" (n = 1,877) or "non-differentially 180 methylated regions" (non-DMRs) (n = 31,182) according to whether or not these regions overlap DM 181 CpG sites (from differential methylation Cluster 3, specifically). We found that hypomethylated regions 182 were significantly enriched for the binding of immune-related TFs relative to regions exhibiting 183 consistent methylation levels. These immune-related TFs include several master regulators of the innate immune response, such as NF-KB/Rel family members NFKB1 (up to 4.6-fold enrichment across the time 184 course (FDR = 4.78×10^{-29})) and RELA (up to 3.6-fold enrichment across the time course (FDR = 1.95×10^{-29})) 185 186 10⁻¹⁸)) Figure 4B; Supplementary Table 5).

We next used CentiDual [5] to test for differential binding of TFs between non-infected and infected samples, specifically focusing on the set of TF family members known to orchestrate innate immune responses to infection (*i.e.*, NF- κ B/Rel, AP-1, STATs, and IRFs). We found increased binding at NF- κ B/Rel binding motifs starting at 2-hours post-infection, despite the fact that no changes in methylation were observed at such early time points (*P* = 0.002; **Figure 4C**; **Supplementary Table 5**; see **Methods**). A similar pattern was observed for AP-1 (*P* = 0.01; **Supplementary Figure 6**). These data show that, while demethylated regions overlap areas bound by immune-induced TFs, the binding of these TFs occurs

196

195

prior to DNA demethylation.

197 Although demethylation does not appear to be required for the binding of key TFs involved in regulation 198 of innate immune responses, it is plausible that the removal of methylation marks at DM sites might 199 enable occupancy of methylation-sensitive factors at later time points [24-26]. In support of this 200 hypothesis, we found that, at later time-points (18 hours and above), there was a stronger enrichment for 201 the binding of TFs that preferentially bind to unmethylated motifs (or "methyl-minus" as defined by Yin et al. [24]) within hypomethylated regions (up to 1.7-fold enrichment; χ^2 -test; $P = 4.14 \times 10^{-34}$; Figure 202 203 **4D**; see **Methods**). Collectively, these results suggest that, although demethylation is likely not required 204 for the engagement of the core regulatory program induced early after infection, it might play a role in 205 fine-tuning the innate immune response by facilitating the binding of salient methyl-sensitive TFs that 206 mediate later immune responses.

207

208 **DISCUSSION**

In this study, we generated paired data on DNA methylation, gene expression, and chromatin accessibility in non-infected and MTB-infected DCs at multiple time-points. Our results show that bacterial infection leads to marked remodeling of the methylome of phagocytic cells (both DCs and macrophages), with several thousand CpG sites showing stable losses of methylation via active DNA demethylation.

Strikingly, in our experiment, virtually all changes in gene expression in response to infection occurred prior to detectable alterations in DNA methylation, suggesting that the observed demethylation is a downstream consequence of TF binding and transcriptional activation. We note, however, that our bisulfite sequencing data does not allow us to distinguish between 5mC and 5hmC. Thus, it is possible that the gain of 5hmC in DM sites, which do not show a loss of 5mC at 2-hours post-infection, precedes the activation of certain enhancers, as was recently suggested in T cells [8].

219

220 The observed changes in methylation most likely occur via TET2-mediated active demethylation, as 221 previously shown [5, 17, 27]. Consistent with this hypothesis, we found that CpG sites that lose 222 methylation upon infection display high levels of 5hmC at baseline, suggesting that these regions are 223 actively bound by TET2 even prior to infection. Moreover, TET2 is strongly upregulated 2 hours after 224 infection (~2.5 fold; Supplementary Figure 7). 5hmC could be a stable intermediate that serves as an epigenetic priming mark, ensuring the rapid response of DCs against infection [19-21, 27-30]. Further 225 226 studies are necessary to investigate the functional relevance of 5hmC in the induction of inflammatory 227 genes during infection.

228

Using footprint analysis, we show that NF-kB/Rel, a master regulator of inflammation, is recruited to 229 230 hypomethylated regions as soon as 2-hours post-infection. This finding is consistent with ChIP-seq data 231 collected from macrophages stimulated with Kdo2-Lipid A (KLA), a highly specific TLR4 agonist, which 232 shows that the NF- κ B subunit p65 is rapidly recruited to enhancer elements within one hour poststimulation [31]. We hypothesize that the rapid binding of NF- κ B, and of other immune-induced TFs, 233 234 instigates chromatin opening which is then followed by the recruitment of histone acetyltransferase p300 235 and the subsequent deposition of activating H3K27ac marks in these regions [32]. Interestingly, p300 can 236 acetylate TET2, conferring enhanced enzyme activity [33], which might account for the eventual loss of 237 DNA methylation in response to infection.

238

239 Our results indicate that most changes in gene expression that occur in response to infection are 240 independent of DNA demethylation, further supporting a lack repressive capacity of DNA methylation 241 [34]. Notably, for only 17 genes—out of thousands of differently expressed genes in response to MTB 242 infection-there is evidence that DNA demethylation occurred prior to gene activation. Similar to 243 previous findings [27, 35-40], our results further reinforce the idea that site-specific regulation of DNA 244 demethylation is mediated by TFs that bind to cis-acting sequences. Interestingly, several recent reports 245 have shown that other epigenetic modifications, such as the H3K4me1 enhancer mark, have a similar passive regulatory function [41-43]. However, our results do not exclude the possibility that 246 247 demethylation might be necessary for the binding of a second wave of TFs that only play a role at later 248 stages of infection (18 hours post-infection or later). In agreement with this hypothesis, we observed a 249 significant enrichment of binding of TFs known to preferentially bind unmethylated CpGs in 250 hypomethylated regions, primarily at later stages post-infection. Ultimately, this suggests that DNA 251 demethylation is not a key regulatory mechanism of early innate immune responses but that it could still 252 play a role in fine-tuning later innate immune responses by facilitating the binding of methylation-253 sensitive TFs at enhancers.

254

255 After an infection is cleared, TFs are expected to unbind, and gene expression as well as DNA 256 methylation levels are anticipated to return to basal state. However, our 72-hour time course study of 257 DNA methylation shows that levels of methylation at DM sites gradually decrease with time post-258 infection and never revert back to higher levels. Interestingly, this pattern is also observed for genes in 259 which the largest fold changes in gene expression occur at earlier time points. Thus, we speculate that 260 demethylation in response to infection could have a specific biological role in innate immune memory 261 [44-47], and that regions that stably lose methylation may act as primed enhancers, potentially allowing 262 for a faster response to a secondary infection.

263

264 METHODS

Biological material and sequencing libraries. Buffy coats from healthy donors were purchased from Indiana Blood Center and all participants signed a written consent. The ethics committee at the CHU Sainte-Justine approved the project (protocol #4023). Peripheral blood mononuclear cells (PBMCs) were obtained by centrifugation on Ficoll-Paque, and monocytes were isolated by positive selection with CD14 magnetic beads (Miltenyi Biotec). Monocytes were differentiated into either DCs by adding rhIL-4 (20 ng/mL; Shenandoah Biotechnology,Inc) and rhGM-CSF (20 ng/mL; R&D Systems Inc.) or macrophages by adding rhM-CSF (20ng/mL; R&D Systems Inc.) in the cell culture medium.

272

DCs were infected with MTB for 2, 18, 48, and 72 h at a multiplicity of infection (MOI) of 1:1 or with heat-killed MTB at MOI of 5:1, as this MOI induces virtually the same transcriptional response at all four time points compared to that observed with live MTB (**Supplementary Figure 2**). Macrophages were infected with *Salmonella typhimurium* as previously described [22]. Briefly, macrophages were infected at MOI of 10:1 for 2 hours, washed, and cultured for 1 hour with 50µg/ml gentamycin, then washed again and cultured in complete medium with 3µg/ml gentamycin for an additional 2, 4, 8, 12, 24 or 48 h, the time points we refer to in the main text.

280

281 DNA from DCs was extracted using the PureGene DNA extraction kit (Gentra Systems). DNA from 282 macrophages was extracted using the DNeasy Blood and Tissue Kit (Qiagen). RNA was extracted using 283 the miRNeasy mini kit (Qiagen). RNA quality was evaluated with the 2100 Bioanalyzer (Agilent 284 Technologies) and only samples with no evidence of RNA degradation (RNA integrity number > 8) were 285 kept for further experiments. RNA-seq libraries were prepared using the TruSeq RNA Sample Prep Kit 286 v2, as per the manufacturer's instructions.

ATAC-seq libraries were generated from 50,000 cells, as previously described [23]. We collected ChIPseq data for the H3K27ac histone mark in non-infected and *Salmonella*-infected macrophages as previously described [5]. Sequencing was performed using the Illumina HiSeq 2500, as per the manufacturer's instructions.

292

293 SeqCap Epi library preparation and sequencing.

294 Libraries were generated with KAPA Library Preparation Kit for Illumina Platforms (KAPA Biosystems), 295 as per the manufacturer's instructions. Briefly, genomic DNA was fragmented to 100-300 bp with an S2 296 sonicator (Covaris). Fragments were then end-repaired, A-tailed, and ligated with methylated sequencing 297 adapters. Between every enzymatic step, libraries were purified using AMPure beads (Agencourt). After 298 ligation, in addition to the AMPure bead purification, a DUAL-SPRI size selection was performed to 299 further select for fragments with adapters in the window of 200-400 bp. Sodium bisulfite conversion was 300 performed with EZ DNA Methylation Lightning Kit (Zymo Research), and libraries were amplified using 301 KAPA Hifi HotStart Uracil Tolerant Enzyme (KAPA Biosystems). Library quality was assessed by 2100 302 Bioanalyzer (Agilent Technologies). Samples showing the desired profile were pooled together in equal 303 mass according to Qubit quantification. We then performed a hybridization using the SeqCap Epi kit 304 (Roche NimbleGen). The sample pool, indexes corresponding to the sequences of the adapters used for 305 library preparation, and repetitive DNA (C_0t) were desiccated and then incubated in hybridization buffer 306 with a set of customized probes for 72 hours to select and sequence target regions only. Specifically, 307 DNA methylation data was collected for 33,059 target regions spanning >130,000 CpG sites (mean length 308 = 300 bp; mean number of CpG sites = 5), which is less than 1% of the \sim 28 million CpGs contained in the 309 human genome. These regions were primarily comprised of MTB-induced differentially methylated 310 regions identified at 18 hours post-infection using whole-genome bisulfite sequencing, as well as other 311 distal regulatory elements in DCs where changes in DNA methylation have been shown to be most likely 312 to occur (Supplementary Figure 1A) [5]. Moreover, these candidate regions were nearby differentially

expressed genes in response to MTB at 18 hours. Probes targeting a two kilobase region between
coordinates 4500 and 6500 bp of the lambda genome (NC_001416.1) were also included in the SeqCap
Epi design, as a control for bisulfite conversion efficiency. Sequencing was performed using the Illumina
HiSeq 2500, as per the manufacturer's instructions.

317

318 SeqCap Epi data processing and differential methylation analysis. Adaptor sequences and low-quality 319 bases (Phred 20) were trimmed Trim score score <first using Galore 320 (http://www.bioinformatics.babraham.ac.uk/projects/trim galore/). The resulting reads were mapped to 321 the human reference genome (GRCh37/hg19) and lambda phage genome using Bismark [48], which uses 322 Bowtie 2 [49] and a bisulfite converted reference genome for read mapping. Only reads that had a unique 323 alignment were retained. Methylation levels for each CpG site were estimated by counting the number of 324 sequenced C ('methylated' reads) divided by the total number of reported C and T ('unmethylated' reads) 325 at the same position of the reference genome using Bismark's methylation extractor tool. We performed a 326 strand-independent analysis of CpG methylation where counts from the two Cs in a CpG and its reverse 327 complement (position i on the plus strand and position i+1 on the minus strand) were combined and 328 assigned to the position of the C in the plus strand. To assess MethylC-seq bisulfite conversion rate, the 329 frequency of unconverted cytosines (C basecalls) at lambda phage CpG reference positions was 330 calculated from reads uniquely mapped to the lambda phage reference genome. Overall, bisulfite 331 conversion rate was >99% in all of the samples (Supplementary Table 1).

332

In DCs, differentially methylated (DM) CpG sites at each time point following MTB infection were identified using the R package DSS [15]. We used a linear model with the following design: DNAmethylation ~ Donor + Infection, which allowed us to consider the paired nature of the experiment and capture the effects of infection on DNA methylation observed within donors. We considered a CpG site as differentially methylated if statistically supported at a False Discovery Rate (FDR) < 0.01 and an absolute mean methylation difference above 10%. Only CpG sites that had a coverage of at least 5X in
each of the samples were included in the analysis (103,649 in total).

340

To identify DM sites that show a stable loss of methylation (as Cluster 3 DM sites in DCs) in *Salmonella*infected macrophages using one individual, we performed a hierarchical clustering analysis on sites that specifically: (*i*) do not change methylation at 2 hours (|methylation difference| < 10%), and (*ii*) lose methylation at 48 hours (methylation difference < -40%).

345

5hmC enrichment at DM sites. To calculate the enrichment of 5-hydroxymethylcytosine (5hmC) at DM CpG sites (Clusters 1, 2 and 3), we compared the distribution of 5hmC levels in non-infected DCs between DM and non-DM sites. Since non-DM sites have lower overall levels of baseline methylation than DM sites (**Supplementary Figure 8A**), we performed similar enrichment analysis by using a random set of non-DM sites that matches the distribution of methylation found in non-infected samples within each set of DM sites (**Supplementary Figure 8B**). Each random set contains the same number of CpG sites as those identified within each DM cluster.

353

RNA-seq data processing and identification of differentially expressed genes. Read count estimates per gene were obtained using the alignment-free method Kallisto [50]. For all downstream analyses, we excluded non-coding and lowly-expressed genes with an average read count lower than 10 in all of the samples, resulting in 13,955 genes in total. The R package DESeq2 [51] was used to identify differences in expression levels between non-infected and infected samples at each time point. Nominal p-values were corrected for multiple testing using the Benjamini-Hochberg method [52]. The complete list of differentially expressed genes can be found in Supplementary Table 3.

Gene set enrichment analysis. We used ClueGO [53] at default parameters to test for enrichment of functionally annotated gene sets among differentially expressed genes. The results for these enrichment analyses are reported in Supplementary Table 4. Enrichment p-values were based on a hypergeometric test using the set of 13,955 genes as background. Benjamini-Hochberg method was applied for multiple testing correction.

367

368 ChIP-seq data processing and tag density profiles. ChIP-seq reads were trimmed for adapter sequences 369 and low-quality score bases using Trim Galore. The resulting reads were mapped to the human reference 370 genome using Bowtie 2 with the following option: -N 1. Only reads that had a unique alignment were 371 retained. and PCR duplicates were further removed using Picard tools 372 (http://broadinstitute.github.io/picard/). Tag density profiles for chromatin modifications and genome 373 accessibility patterns around regions of interest were accomplished with ngs.plot package [54] using 374 default parameters.

375

376 ATAC-seq data processing and TF footprinting analysis. ATAC-seq reads were trimmed for adapter 377 sequences and low-quality score bases and were mapped to the human reference genome. Mapping was 378 performed using BWA-MEM [55] in paired-end mode at default parameters. Only reads that had a unique 379 alignment (mapping quality > 10) were retained. TF footprinting analyses were performed as previously 380 described, using the Centidual algorithm [5] and JASPAR annotated human TF binding motifs (2018 381 release) [56]. For each of the actively bound TFs in DCs (241 in total; FDR < 0.05 at 18 hours post-382 infection; **Supplementary Table 5**)), we first trained Centidual assuming that the footprint was bound in 383 the two conditions. Then, we fixed the model parameters and generated a likelihood ratio and posterior probability π_{lt} for each condition t separately and for each site l. To detect if the footprint was more 384 385 active in one of the two conditions, we fit a logistic model that included an intercept for each condition (α and δ), the PWM effect β , and PWM times the treatment effect γ : 386

$$\log\left(\frac{\pi_{lt}}{1-\pi_{lt}}\right) = \alpha \times (1-I_t) + \beta \times \text{PWMscore}_t + \delta \times I_t + \gamma \times (I_t \times \text{PWMscore}_t)$$
387

where I_t is an indicator variable that takes the value 1 if t = "treatment" and 0 if t = "control". We then calculated a Z-score for the interaction effect γ , corresponding to the evidence for condition-specific binding. ATAC-seq samples were down-sampled to obtain similar number of reads between NI and HI samples at each time-point. We used a window size of 300 bp on either side of the motif match, and reads with fragment lengths [40, 140] and [141, 600] bp for footprinting analyses.

393

To test for differential binding of immune-related TFs (NF- κ B/Rel, AP-1, STATs, and IRFs) between non-infected and infected samples, we compared the intensity of the Tn5 sensitivity-based footprint across all matches to motifs of TFs that belong to each family in the hypomethylated regions. Specifically, the following motif IDs (and corresponding names) were aggregated to their respective TF family:

NF-к	B/Rel
MA0105.3	NFKB1
MA0105.2	NFKB1
MA0105.1	NFKB1
MA0105.4	NFKB1
MA0778.1	NFKB2
MA0101.1	REL
MA0107.1	RELA
MA1117.1	RELB

MA0833.1 ATF4 MA0833.1 ATF7 MA0834.1 BATF7 MA0462.1 BATF3 MA0462.1 BATF3 MA0462.1 BATF3 MA0462.1 BATF3 MA0476.1 FOS MA0099.3 FOS::JUN MA1126.1 FOS::JUN(var.2) MA1134.1 FOS::JUNB MA1141.1 FOS::JUND MA1141.1 FOS::JUND MA1135.1 FOSB::JUNB MA1135.1 FOSB::JUNB(var.2) MA1136.1 FOSB::JUNB(var.2) MA1136.1 FOSL1::JUND(var.2) MA1128.1 FOSL1::JUND MA1129.1 FOSL1::JUND MA1137.1 FOSL1::JUND MA1142.1 FOSL1::JUND MA1142.1 FOSL1::JUND MA1142.1 FOSL1::JUND MA1143.1 FOSL2::JUND	AP-1				
MA0834.1 ATF7 MA0462.1 BATF::JUN MA0462.1 BATF::JUN MA0835.1 BATF3 MA0476.1 FOS MA0099.3 FOS::JUN MA1126.1 FOS::JUNB MA1134.1 FOS::JUND MA1141.1 FOS::JUNB MA1127.1 FOSB::JUNB MA1135.1 FOSB::JUNB(var.2) MA1136.1 FOSL1::JUNB(var.2) MA1128.1 FOSL1::JUNN MA1129.1 FOSL1::JUND(var.2) MA1137.1 FOSL1::JUND(var.2) MA1142.1 FOSL2::JUND MA1142.1 FOSL2::JUN MA1130.1 FOSL2::JUN MA1131.1 FOSL2::JUNB MA1131.1 FOSL2::JUNB(var.2) MA1138.1 FOSL2::JUNB(var.2) MA1139.1 FOSL2::JUNB(v	MA0833.1				
MA0835.1 BATF3 MA0476.1 FOS MA0099.3 FOS::JUN MA1126.1 FOS::JUN(var.2) MA1126.1 FOS::JUN(var.2) MA1134.1 FOS::JUNB MA1141.1 FOS::JUND MA1141.1 FOS::JUND MA1135.1 FOSB::JUNB MA1135.1 FOSB::JUNB MA1135.1 FOSB::JUNB MA1135.1 FOSB::JUNB MA1135.1 FOSB::JUNB(var.2) MA1136.1 FOSL1::JUNB(var.2) MA1128.1 FOSL1::JUNN MA1129.1 FOSL1::JUND(var.2) MA1137.1 FOSL1::JUND MA1142.1 FOSL1::JUND(var.2) MA1137.1 FOSL2::JUND MA1130.1 FOSL2::JUND MA1131.1 FOSL2::JUN MA1131.1 FOSL2::JUNB MA1139.1 FOSL2::JUNB(var.2) MA1139.1 FOSL2::JUNB(var.2)		ATF7			
MA0476.1 FOS MA0099.3 FOS::JUN MA126.1 FOS::JUN(var.2) MA1126.1 FOS::JUNB MA1134.1 FOS::JUNB MA1134.1 FOS::JUND MA1134.1 FOS::JUND MA1134.1 FOS::JUND MA1135.1 FOSB::JUNB MA1135.1 FOSB::JUNB MA1135.1 FOSB::JUNB MA1135.1 FOSB::JUNB MA1135.1 FOSB::JUNB MA1135.1 FOSL1::JUNB MA1128.1 FOSL1::JUN MA1129.1 FOSL1::JUND MA1137.1 FOSL1::JUND MA1142.1 FOSL1::JUND MA1142.1 FOSL1::JUND MA1143.1 FOSL2::JUND MA1130.1 FOSL2::JUN MA1131.1 FOSL2::JUNB MA1131.1 FOSL2::JUNB MA1139.1 FOSL2::JUNB(var.2) MA1139.1 FOSL2::JUNB(var.2)	MA0462.1	BATF::JUN			
MA0099.3 FOS::JUN MA1126.1 FOS::JUN(var.2) MA1126.1 FOS::JUNB MA1134.1 FOS::JUNB MA1134.1 FOS::JUND MA1134.1 FOS::JUND MA1135.1 FOSB::JUNB MA1135.1 FOSB::JUNB MA1135.1 FOSB::JUNB(var.2) MA1135.1 FOSB::JUNB(var.2) MA1136.1 FOSB::JUNB(var.2) MA0477.1 FOSL1 MA1128.1 FOSL1::JUN MA1129.1 FOSL1::JUNN MA1137.1 FOSL1::JUND MA1137.1 FOSL1::JUND MA1142.1 FOSL1::JUND MA1143.1 FOSL2::JUND MA1130.1 FOSL2::JUN MA1131.1 FOSL2::JUN MA1131.1 FOSL2::JUNB MA1139.1 FOSL2::JUNB(var.2) MA1139.1 FOSL2::JUNB(var.2) MA1139.1 FOSL2::JUNB(var.2)	MA0835.1	BATF3			
MA1126.1 FOS::JUN(var.2) MA1134.1 FOS::JUNB MA1134.1 FOS::JUND MA1134.1 FOS::JUND MA1141.1 FOS::JUND MA1127.1 FOSB::JUN MA1135.1 FOSB::JUNB MA1135.1 FOSB::JUNB MA1135.1 FOSB::JUNB MA1135.1 FOSB::JUNB(var.2) MA1136.1 FOSL1::JUNB(var.2) MA1129.1 FOSL1::JUNV(var.2) MA1142.1 FOSL1::JUND MA1142.1 FOSL1::JUND MA1143.1 FOSL1::JUND(var.2) MA1143.1 FOSL2::JUND MA1130.1 FOSL2::JUN MA1131.1 FOSL2::JUNB MA1131.1 FOSL2::JUNB MA1139.1 FOSL2::JUNB(var.2) MA1139.1 FOSL2::JUNB(var.2)	MA0476.1	FOS			
MA1134.1 FOS::JUNB MA1134.1 FOS::JUND MA1141.1 FOS::JUND MA1127.1 FOSB::JUN MA1135.1 FOSB::JUNB MA1135.1 FOSB::JUNB MA1135.1 FOSB::JUNB MA1135.1 FOSB::JUNB MA1135.1 FOSB::JUNB MA1136.1 FOSB::JUNB(var.2) MA0477.1 FOSL1 MA1128.1 FOSL1::JUN MA1129.1 FOSL1::JUNN(var.2) MA1137.1 FOSL1::JUND MA1142.1 FOSL1::JUND(var.2) MA1143.1 FOSL2::JUND MA1130.1 FOSL2::JUN MA1131.1 FOSL2::JUNB MA1138.1 FOSL2::JUNB MA1139.1 FOSL2::JUNB(var.2) MA1139.1 FOSL2::JUNB(var.2) MA1139.1 FOSL2::JUNB(var.2)	MA0099.3	FOS::JUN			
MA1141.1 FOS::JUND MA1127.1 FOSB::JUN MA1135.1 FOSB::JUNB MA1135.1 FOSB::JUNB MA1136.1 FOSB::JUNB(var.2) MA0477.1 FOSL1 MA1128.1 FOSL1::JUN MA1129.1 FOSL1::JUN(var.2) MA1137.1 FOSL1::JUND MA1142.1 FOSL1::JUND MA1143.1 FOSL1::JUND(var.2) MA1143.1 FOSL2::JUND MA1130.1 FOSL2::JUN MA1131.1 FOSL2::JUN MA1138.1 FOSL2::JUNB MA1139.1 FOSL2::JUNB(var.2) MA1139.1 FOSL2::JUNB(var.2)	MA1126.1	FOS::JUN(var.2)			
MA1127.1 FOSB::JUN MA1135.1 FOSB::JUNB MA1135.1 FOSB::JUNB MA1136.1 FOSB::JUNB(var.2) MA0477.1 FOSL1 MA1128.1 FOSL1::JUN MA1129.1 FOSL1::JUN(var.2) MA1137.1 FOSL1::JUNB MA1142.1 FOSL1::JUND MA1143.1 FOSL1::JUND(var.2) MA1143.1 FOSL2::JUND MA1130.1 FOSL2::JUN MA1131.1 FOSL2::JUNB MA1138.1 FOSL2::JUNB MA1139.1 FOSL2::JUNB MA1139.1 FOSL2::JUNB MA1139.1 FOSL2::JUNB	MA1134.1	FOS::JUNB			
MA1135.1 FOSB::JUNB MA1136.1 FOSB::JUNB(var.2) MA0477.1 FOSL1 MA1128.1 FOSL1::JUN MA1129.1 FOSL1::JUN(var.2) MA1137.1 FOSL1::JUNB MA1142.1 FOSL1::JUND MA1142.1 FOSL1::JUND MA1143.1 FOSL1::JUND(var.2) MA1143.1 FOSL2::JUND MA1130.1 FOSL2::JUN MA1131.1 FOSL2::JUN MA1138.1 FOSL2::JUNB MA1139.1 FOSL2::JUNB(var.2) MA1139.1 FOSL2::JUNB(var.2) MA1139.1 FOSL2::JUNB(var.2)	MA1141.1	FOS::JUND			
MA1136.1 FOSB::JUNB(var.2) MA0477.1 FOSL1 MA1128.1 FOSL1::JUN MA1129.1 FOSL1::JUN MA1129.1 FOSL1::JUN(var.2) MA1137.1 FOSL1::JUNB MA1142.1 FOSL1::JUND MA1142.1 FOSL1::JUND(var.2) MA1143.1 FOSL1::JUND(var.2) MA1130.1 FOSL2::JUN MA1131.1 FOSL2::JUN MA1138.1 FOSL2::JUNB MA1139.1 FOSL2::JUNB(var.2) MA1139.1 FOSL2::JUNB(var.2) MA1139.1 FOSL2::JUNB(var.2)	MA1127.1	FOSB::JUN			
MA0477.1 FOSL1 MA1128.1 FOSL1::JUN MA1129.1 FOSL1::JUN(var.2) MA1137.1 FOSL1::JUND MA1142.1 FOSL1::JUND MA1142.1 FOSL1::JUND MA1142.1 FOSL1::JUND MA1142.1 FOSL1::JUND(var.2) MA1143.1 FOSL2::JUND(var.2) MA1130.1 FOSL2::JUNN MA1131.1 FOSL2::JUNB MA1138.1 FOSL2::JUNB MA1139.1 FOSL2::JUNB(var.2) MA1139.1 FOSL2::JUNB(var.2)	MA1135.1				
MA1128.1 FOSL1::JUN MA1129.1 FOSL1::JUN(var.2) MA1129.1 FOSL1::JUN(var.2) MA1137.1 FOSL1::JUND MA1142.1 FOSL1::JUND MA1142.1 FOSL1::JUND MA1142.1 FOSL1::JUND MA1143.1 FOSL1::JUND(var.2) MA0478.1 FOSL2::JUN MA1130.1 FOSL2::JUN MA1131.1 FOSL2::JUNN(var.2) MA1138.1 FOSL2::JUNB MA1139.1 FOSL2::JUNB(var.2) MA1134.1 FOSL2::JUNB(var.2)	MA1136.1	FOSB::JUNB(var.2)			
MA1129.1 FOSL1::JUN(var.2) MA1137.1 FOSL1::JUNB MA1137.1 FOSL1::JUND MA1142.1 FOSL1::JUND MA1142.1 FOSL1::JUND MA1142.1 FOSL1::JUND MA1143.1 FOSL1::JUND(var.2) MA0478.1 FOSL2 MA1130.1 FOSL2::JUN MA1131.1 FOSL2::JUNN MA1138.1 FOSL2::JUNB MA1139.1 FOSL2::JUNB(var.2) MA1139.1 FOSL2::JUND	MA0477.1	FOSL1			
MA1137.1 FOSL1::JUNB MA1142.1 FOSL1::JUND MA1143.1 FOSL1::JUND(var.2 MA0478.1 FOSL2 MA1130.1 FOSL2::JUN MA1131.1 FOSL2::JUN(var.2) MA1138.1 FOSL2::JUNB MA1139.1 FOSL2::JUNB MA1139.1 FOSL2::JUNB(var.2) MA1139.1 FOSL2::JUNB(var.2)	MA1128.1				
MA1142.1 FOSL1::JUND MA1143.1 FOSL1::JUND(var.2 MA0478.1 FOSL2 MA1130.1 FOSL2::JUN MA1131.1 FOSL2::JUN(var.2) MA1138.1 FOSL2::JUNB MA1139.1 FOSL2::JUNB MA1139.1 FOSL2::JUNB(var.2) MA1139.1 FOSL2::JUNB(var.2)	MA1129.1	FOSL1::JUN(var.2)			
MA1143.1 FOSL1::JUND(var.2 MA0478.1 FOSL2 MA1130.1 FOSL2::JUN MA1131.1 FOSL2::JUN(var.2) MA1138.1 FOSL2::JUNB MA1139.1 FOSL2::JUNB(var.2) MA1139.1 FOSL2::JUNB(var.2) MA1144.1 FOSL2::JUND	-	FOSL1::JUNB			
MA0478.1 FOSL2 MA1130.1 FOSL2::JUN MA1131.1 FOSL2::JUN(var.2) MA1138.1 FOSL2::JUNB MA1139.1 FOSL2::JUNB(var.2) MA1139.1 FOSL2::JUNB(var.2) MA1144.1 FOSL2::JUND	MA1142.1	FOSL1::JUND			
MA1130.1 FOSL2::JUN MA1131.1 FOSL2::JUN(var.2) MA1138.1 FOSL2::JUNB MA1139.1 FOSL2::JUNB(var.2) MA1139.1 FOSL2::JUNB(var.2) MA1144.1 FOSL2::JUND	MA1143.1	FOSL1::JUND(var.2)			
MA1131.1 FOSL2::JUN(var.2) MA1138.1 FOSL2::JUNB MA1139.1 FOSL2::JUNB(var.2) MA1144.1 FOSL2::JUND	MA0478.1	FOSL2			
MA1138.1 FOSL2::JUNB MA1139.1 FOSL2::JUNB(var.2) MA1144.1 FOSL2::JUND	MA1130.1	FOSL2::JUN			
MA1139.1 FOSL2::JUNB(var.2 MA1144.1 FOSL2::JUND	MA1131.1	FOSL2::JUN(var.2)			
MA1144.1 FOSL2::JUND	MA1138.1				
MA1145.1 FOSL2::JUND(var.2					
	-				
MA0655.1 JDP2		-			
MA0656.1 JDP2(var.2)	MA0656.1	JDP2(var.2)			
MA0488.1 JUN					
MA0489.1 JUN(var.2)					
MA1132.1 JUN::JUNB	MA1132.1				
MA1133.1 JUN::JUNB(var.2)					
MA0490.1 JUNB					
MA1140.1 JUNB(var.2)	-	. ,			
MA0491.1 JUND	MA0491.1	JUND			

STATs						
MA0137.1	STAT1					
MA0137.2	STAT1					
MA0137.3	STAT1					
MA0517.1	STAT1::STAT2					
MA0144.2	STAT3					
MA0144.2	STAT3					

IR	Fs
MA0050.2	IRF1
MA0050.1	IRF1
MA0051.1	IRF2
MA1418.1	IRF3
MA1419.1	IRF4
MA1420.1	IRF5
MA0772.1	IRF7
MA0652.1	IRF8
MA0653.1	IRF9

400

401 To test for enrichment of binding of methylation-sensitive ("methyl-minus") TFs in hypomethylated 402 regions, we compared the proportion of regions that overlap well-supported footprints (posterior 403 probability > 0.99) of "methyl-minus" TFs reported in Yin *et al.* [24]) among non-DMRs and 404 hypomethylated regions (with 250-bp flanking the start and end). The list of motif IDs (and 405 corresponding names) that were included in the analysis are shown below:

MA0018.1	CREB1	MA0495.2	MAFF	MA0823.1	HEY1
MA0018.3	CREB1	MA0511.2	RUNX2	MA0830.1	TCF4
MA0028.2	ELK1	MA0526.1	USF2	MA0831.1	TFE3
MA0058.1	MAX	MA0526.2	USF2	MA0831.2	TFE3
MA0058.3	MAX	MA0636.1	BHLHE41	MA0834.1	ATF7
MA0059.1	MAX::MYC	MA0638.1	CREB3	MA0835.1	BATF3
MA0062.1	GABPA	MA0640.1	ELF3	MA0839.1	CREB3L1
MA0093.2	USF1	MA0641.1	ELF4	MA0871.1	TFEC
MA0095.1	YY1	MA0649.1	HEY2	MA1126.1	FOS::JUN(var.2)
MA0095.2	YY1	MA0663.1	MLX	MA1127.1	FOSB::JUN
MA0099.3	FOS::JUN	MA0664.1	MLXIPL	MA1128.1	FOSL1::JUN
MA0104.4	MYCN	MA0736.1	GLIS2	MA1129.1	FOSL1::JUN(var.2)
MA0136.2	ELF5	MA0749.1	ZBED1	MA1130.1	FOSL2::JUN
MA0149.1	EWSR1-FLI1	MA0750.1	ZBTB7A	MA1131.1	FOSL2::JUN(var.2)
MA0156.2	FEV	MA0750.2	ZBTB7A	MA1134.1	FOS::JUNB
MA0464.2	BHLHE40	MA0757.1	ONECUT3	MA1135.1	FOSB::JUNB
MA0470.1	E2F4	MA0759.1	ELK3	MA1136.1	FOSB::JUNB(var.2)
MA0473.1	ELF1	MA0761.1	ETV1	MA1137.1	FOSL1::JUNB
MA0473.2	ELF1	MA0762.1	ETV2	MA1138.1	FOSL2::JUNB
MA0474.2	ERG	MA0763.1	ETV3	MA1139.1	FOSL2::JUNB(var.2)
MA0475.1	FLI1	MA0764.1	ETV4	MA1141.1	FOS::JUND
MA0475.2	FLI1	MA0765.1	ETV5	MA1142.1	FOSL1::JUND
MA0476.1	FOS	MA0772.1	IRF7	MA1143.1	FOSL1::JUND(var.2)
MA0477.1	FOSL1	MA0821.1	HES5	MA1144.1	FOSL2::JUND
MA0478.1	FOSL2	MA0822.1	HES7	MA1145.1	FOSL2::JUND(var.2)

406

407

408 Relationship between gene expression and chromatin accessibility. Peaks were first called on ATAC-409 seq using the MACS2 software suite [57] with the added parameters: -g hs -q 0.05 --broad --nomodel --410 extsize 200 --nolambda. All peaks from each sample were then merged to provide one set of combined 411 peaks. To count the number of reads overlapping peaks, we used featureCount (from the subread 412 package) [58] with the following option: -p -P. For all downstream analyses, we excluded low-count 413 peaks with an average read count lower than 10 across all samples, resulting in 79,282 peaks in total. We 414 then plotted the distribution of changes in Tn5 accessibility (between non-infected and MTB-infected 415 DCs across the five time-points of infection (2, 4, 18, 24, 48, and 72 hours)) for the top 25% most 416 variable peaks associated with DE genes in each cluster. The DE genes associated with the selected peaks 417 represent ~50% of the total genes within each of the DE clusters: (i) Early induced: 418/765 = 55%; (ii) 418 Intermediate induced: 418/839 = 49%; and (*iii*) Persistent induced: 1083/2091 = 52%.

419

420 DATA ACCESS

- 421 Data generated in this study have been submitted to the NCBI Gene Expression Omnibus
 422 (GEO; <u>http://www.ncbi.nlm.nih.gov/geo/</u>) under accession numbers GSE116406 (ATAC-
- 423 seq), GSE116411 (ChIP-seq), GSE116405 (RNA-seq), and GSE116399 (SeqCap Epi)

424

425 ACKNOWLEDGMENTS

We thank Calcul Quebec and Compute Canada for managing and providing access to the supercomputer
Briaree from the University of Montreal. This study was funded by grants from the Canadian Institutes of
Health Research (301538 and 232519), and the Canada Research Chairs Program (950-228993) (to
L.B.B.). A.P. and F.M-L. were supported by a fellowship from the The Fonds de recherche du Québec –
Santé (FRQS).

431

432 COMPETING INTEREST STATEMENT

433 The authors declare no competing financial interests.

434

435 FIGURE LEGENDS

Figure 1. (A) Barplots showing the number of differentially methylated (DM) CpG sites identified at a 436 437 |methylation difference| > 10% and FDR < 0.01 (y-axis) at each time point after MTB infection (2, 18, 48, 438 and 72 hours (h)) (x-axis). (B) Distribution of differences in methylation between infected and non-439 infected cells at DM sites, at each time point. (C) Heatmap of differences in methylation constructed 440 using unsupervised hierarchical clustering of the 4,578 DM sites (identified at any time point using live 441 and heat-inactivated MTB-infected samples combined; y-axis) across four time points after infection, 442 which shows three distinct patterns of changes in methylation. (D) Mean differences in methylation of 443 CpG sites in each cluster across all time points; shading denotes ± 1 standard deviation. For visualization

purposes, we also show the '0h' time point, where we expect no changes in methylation. (E) Boxplots
comparing the distribution of 5hmC levels in non-infected DCs between non-DM and DM sites (Cluster
3).

447

448 Figure 2. (A) Heatmap of differences in expression (standardized log2 fold changes) constructed using 449 unsupervised hierarchical clustering of the 7,457 differentially expressed genes (identified at any time 450 point using cutoffs of $|\log 2FC| > 1$ and FDR < 0.01; y-axis) across four time points after MTB infection 451 results in six distinct patterns of changes in expression. (B) Mean log2 fold expression changes of genes 452 in each cluster across all time points; shading denotes ± 1 standard deviation. For visualization purposes, 453 we also show the '0h' time point, where we expect no changes in expression. (C) Gene ontology 454 enrichment analyses among genes that are repressed or induced in response to MTB infection. (D) 455 Enrichment (in log2; x-axis) of differentially expressed genes associated with differentially methylated 456 CpG sites (Cluster 3). Error bars show 95% confidence intervals for the enrichment estimates. (E) 457 Boxplots showing the distribution of standardized differences in methylation of DM sites in Cluster 3 458 (blue) along with the corresponding standardized differences in expression of the associated genes 459 (orange), across all time points.

460

Figure 3. (A) Mean differences in methylation (y-axis) in CpG sites that show stable losses of 461 462 methylation (similar to Cluster 3 DM sites in Figure 1C,D; n = 453) in Salmonella-infected macrophages, 463 across six time points after infection (2, 4, 8, 12, 24, and 48 hours (h); x-axis). Shading denotes ± 1 464 standard deviation. For visualization purposes, we also show the '0h' time point, where we expect no changes in methylation. (B) Composite plots of patterns of H3K27ac ChIP-seq signals ± 5 kb around the 465 466 midpoints of hypomethylated sites (x-axis) in macrophages at 2 hours post-infection with Salmonella. (C) 467 Distribution of log2 fold expression changes (between non-infected and Salmonella-infected macrophages 468 at 2 hours) for genes associated with DM sites in Figure 3A (n = 269).

469

470 Figure 4. (A) Boxplots showing the distribution of log2 fold changes in chromatin accessibility between non-infected and MTB-infected DCs across the five time points of infection (2, 4, 18, 24, 48, and 72 471 472 hours) for open chromatin regions associated with the three classes of induced genes described in Figure 473 2A,B. (B) TF binding motifs for which the number of well-supported footprints (posterior probability >(0.99) within hypomethylated regions were enriched (FDR < 0.01) relative to non-DMRs (with 250-bp 474 475 flanking the start and end) in MTB-infected DCs. The enrichment factors (x-axis) are shown in a log2 scale and error bars reflect the 95% confidence intervals. A complete list of all TF binding motifs for 476 477 which footprints are enriched within hypomethylated regions can be found in Supplementary Table 5. (C) 478 Barplots showing significant differences in TF occupancy score predictions for NF-KB/Rel motifs 479 between MTB-infected and non-infected DCs (Z_{MTB} - Z_{NI}; y-axis; see Methods) across all time points (x-480 axis). A positive Z-score difference indicates increased TF binding in hypomethylated regions after MTB 481 infection. (**D**) Proportion of regions that overlap a methylation-sensitive ("methyl-minus"; reported in Yin 482 et al. [24]) TF footprint (y-axis) observed among non-DMRs and hypomethylated regions (or hypo-483 DMRs; see Methods).

485 **REFERENCES**

- Medzhitov R, Horng T: Transcriptional control of the inflammatory response. Nat Rev
 Immunol 2009, 9:692-703.
- 488 2. Smale ST: Selective transcription in response to an inflammatory stimulus. *Cell* 2010,
 489 140:833-844.
- 490 3. Smale ST, Tarakhovsky A, Natoli G: Chromatin contributions to the regulation of innate
 491 immunity. Annu Rev Immunol 2014, 32:489-511.
- 492 4. Bierne H, Hamon M, Cossart P: Epigenetics and bacterial infections. Cold Spring Harb
 493 Perspect Med 2012, 2:a010272.
- 494 5. Pacis A, Tailleux L, Morin AM, Lambourne J, MacIsaac JL, Yotova V, Dumaine A, Danckaert
- 495 A, Luca F, Grenier JC, et al: Bacterial infection remodels the DNA methylation landscape of
 496 human dendritic cells. *Genome Res* 2015.
- 497 6. Marr AK, MacIsaac JL, Jiang R, Airo AM, Kobor MS, McMaster WR: Leishmania donovani
- 498 Infection Causes Distinct Epigenetic DNA Methylation Changes in Host Macrophages. *PLoS* 499 *Pathog* 2014, 10:e1004419.
- 500 7. Bruniquel D, Schwartz RH: Selective, stable demethylation of the interleukin-2 gene enhances
 501 transcription by an active process. *Nat Immunol* 2003, 4:235-240.
- 502 8. Ichiyama K, Chen T, Wang X, Yan X, Kim BS, Tanaka S, Ndiaye-Lobry D, Deng Y, Zou Y,
- 503Zheng P, et al: The methylcytosine dioxygenase Tet2 promotes DNA demethylation and504activation of cytokine gene expression in T cells. Immunity 2015, 42:613-626.
- Murayama A, Sakura K, Nakama M, Yasuzawa-Tanaka K, Fujita E, Tateishi Y, Wang Y,
 Ushijima T, Baba T, Shibuya K, et al: A specific CpG site demethylation in the human
 interleukin 2 gene promoter is an epigenetic memory. *EMBO J* 2006, 25:1081-1092.

- 508 10. Sinclair SH, Yegnasubramanian S, Dumler JS: Global DNA methylation changes and
 509 differential gene expression in Anaplasma phagocytophilum-infected human neutrophils.
 510 Clin Epigenetics 2015, 7:77.
- 511 11. Wiencke JK, Butler R, Hsuang G, Eliot M, Kim S, Sepulveda MA, Siegel D, Houseman EA,
 512 Kelsey KT: The DNA methylation profile of activated human natural killer cells. *Epigenetics*
- 513 2016, **11:**363-380.
- 514 12. Zhang X, Ulm A, Somineni HK, Oh S, Weirauch MT, Zhang HX, Chen X, Lehn MA, Janssen
 515 EM, Ji H: DNA methylation dynamics during ex vivo differentiation and maturation of
 516 human dendritic cells. *Epigenetics Chromatin* 2014, 7:21.
- 517 13. Cizmeci D, Dempster EL, Champion OL, Wagley S, Akman OE, Prior JL, Soyer OS, Mill J,
 518 Titball RW: Mapping epigenetic changes to the host cell genome induced by Burkholderia
 519 pseudomallei reveals pathogen-specific and pathogen-generic signatures of infection. Sci
 520 Rep 2016, 6:30861.
- Heintzman ND, Hon GC, Hawkins RD, Kheradpour P, Stark A, Harp LF, Ye Z, Lee LK, Stuart
 RK, Ching CW, et al: Histone modifications at human enhancers reflect global cell-typespecific gene expression. *Nature* 2009, 459:108-112.
- 524 15. Feng H, Conneely KN, Wu H: A Bayesian hierarchical model to detect differentially
 525 methylated loci from single nucleotide resolution sequencing data. Nucleic Acids Res 2014,
 526 42:e69.
- 527 16. Wu X, Zhang Y: TET-mediated active DNA demethylation: mechanism, function and
 528 beyond. Nat Rev Genet 2017, 18:517-534.
- 529 17. Klug M, Schmidhofer S, Gebhard C, Andreesen R, Rehli M: 5-Hydroxymethylcytosine is an
 530 essential intermediate of active DNA demethylation processes in primary human
 531 monocytes. *Genome Biol* 2013, 14:R46.

- Alvarez-Errico D, Vento-Tormo R, Sieweke M, Ballestar E: Epigenetic control of myeloid cell
 differentiation, identity and function. *Nat Rev Immunol* 2015, 15:7-17.
- 19. Mahe EA, Madigou T, Serandour AA, Bizot M, Avner S, Chalmel F, Palierne G, Metivier R,
- Salbert G: Cytosine modifications modulate the chromatin architecture of transcriptional
 enhancers. Genome Res 2017, 27:947-958.
- 537 20. Yu M, Hon GC, Szulwach KE, Song CX, Zhang L, Kim A, Li X, Dai Q, Shen Y, Park B, et al:
 538 Base-resolution analysis of 5-hydroxymethylcytosine in the mammalian genome. *Cell* 2012,
- **149:**1368-1380.
- 540 21. Calo E, Wysocka J: Modification of enhancer chromatin: what, how, and why? *Mol Cell*541 2013, 49:825-837.
- 542 22. Nedelec Y, Sanz J, Baharian G, Szpiech ZA, Pacis A, Dumaine A, Grenier JC, Freiman A, Sams
 543 AJ, Hebert S, et al: Genetic Ancestry and Natural Selection Drive Population Differences in
 544 Immune Responses to Pathogens. *Cell* 2016, 167:657-669 e621.
- 545 23. Buenrostro JD, Giresi PG, Zaba LC, Chang HY, Greenleaf WJ: Transposition of native
 546 chromatin for fast and sensitive epigenomic profiling of open chromatin, DNA-binding
 547 proteins and nucleosome position. *Nat Methods* 2013, 10:1213-1218.
- 548 24. Yin Y, Morgunova E, Jolma A, Kaasinen E, Sahu B, Khund-Sayeed S, Das PK, Kivioja T, Dave
 549 K, Zhong F, et al: Impact of cytosine methylation on DNA binding specificities of human
 550 transcription factors. *Science* 2017, 356.
- 551 25. Domcke S, Bardet AF, Adrian Ginno P, Hartl D, Burger L, Schubeler D: Competition between
 552 DNA methylation and transcription factors determines binding of NRF1. *Nature* 2015,
 553 528:575-579.
- Zhu H, Wang G, Qian J: Transcription factors as readers and effectors of DNA methylation. *Nat Rev Genet* 2016, 17:551-565.

556	27.	Vento-Tormo R, Company C, Rodriguez-Ubreva J, de la Rica L, Urquiza JM, Javierre BM,
557		Sabarinathan R, Luque A, Esteller M, Aran JM, et al: IL-4 orchestrates STAT6-mediated DNA
558		demethylation leading to dendritic cell differentiation. Genome Biol 2016, 17:4.
559	28.	Serandour AA, Avner S, Oger F, Bizot M, Percevault F, Lucchetti-Miganeh C, Palierne G,
560		Gheeraert C, Barloy-Hubler F, Peron CL, et al: Dynamic hydroxymethylation of
561		deoxyribonucleic acid marks differentiation-associated enhancers. Nucleic Acids Res 2012,
562		40: 8255-8265.
563	29.	Hon GC, Song CX, Du T, Jin F, Selvaraj S, Lee AY, Yen CA, Ye Z, Mao SQ, Wang BA, et al:
564		5mC Oxidation by Tet2 Modulates Enhancer Activity and Timing of Transcriptome
565		Reprogramming during Differentiation. Mol Cell 2014.
566	30.	Creyghton MP, Cheng AW, Welstead GG, Kooistra T, Carey BW, Steine EJ, Hanna J, Lodato
567		MA, Frampton GM, Sharp PA, et al: Histone H3K27ac separates active from poised
568		enhancers and predicts developmental state. Proc Natl Acad Sci U S A 2010, 107:21931-
569		21936.
570	31.	Kaikkonen MU, Spann NJ, Heinz S, Romanoski CE, Allison KA, Stender JD, Chun HB, Tough
571		DF, Prinjha RK, Benner C, Glass CK: Remodeling of the enhancer landscape during
572		macrophage activation is coupled to enhancer transcription. <i>Mol Cell</i> 2013, 51: 310-325.
573	32.	Bhatt D, Ghosh S: Regulation of the NF-kappaB-Mediated Transcription of Inflammatory
574		Genes. Front Immunol 2014, 5:71.
575	33.	Zhang YW, Wang Z, Xie W, Cai Y, Xia L, Easwaran H, Luo J, Yen RC, Li Y, Baylin SB:
576		Acetylation Enhances TET2 Function in Protecting against Abnormal DNA Methylation
577		during Oxidative Stress. Mol Cell 2017, 65:323-335.
578	34.	Ford EE, Grimmer MR, Stolzenburg S, Bogdanovic O, de Mendoza A, Farnham PJ, Blancafort P,
579		Lister R: Frequent lack of repressive capacity of promoter DNA methylation identified
580		through genome-wide epigenomic manipulation. bioRxiv 2017.

- 581 35. Stadler MB, Murr R, Burger L, Ivanek R, Lienert F, Scholer A, van Nimwegen E, Wirbelauer C,
- 582 Oakeley EJ, Gaidatzis D, et al: **DNA-binding factors shape the mouse methylome at distal** 583 regulatory regions. *Nature* 2011, **480**:490-495.
- 36. Han L, Lin IG, Hsieh CL: Protein binding protects sites on stable episomes and in the
 chromosome from de novo methylation. *Mol Cell Biol* 2001, 21:3416-3424.
- 586 37. Kress C, Thomassin H, Grange T: Active cytosine demethylation triggered by a nuclear
 587 receptor involves DNA strand breaks. *Proc Natl Acad Sci U S A* 2006, 103:11112-11117.
- 588 38. Sato N, Kondo M, Arai K: The orphan nuclear receptor GCNF recruits DNA
 589 methyltransferase for Oct-3/4 silencing. *Biochem Biophys Res Commun* 2006, 344:845-851.
- Schubeler D: Function and information content of DNA methylation. *Nature* 2015, 517:321326.
- 40. de la Rica L, Rodriguez-Ubreva J, Garcia M, Islam AB, Urquiza JM, Hernando H, Christensen J,

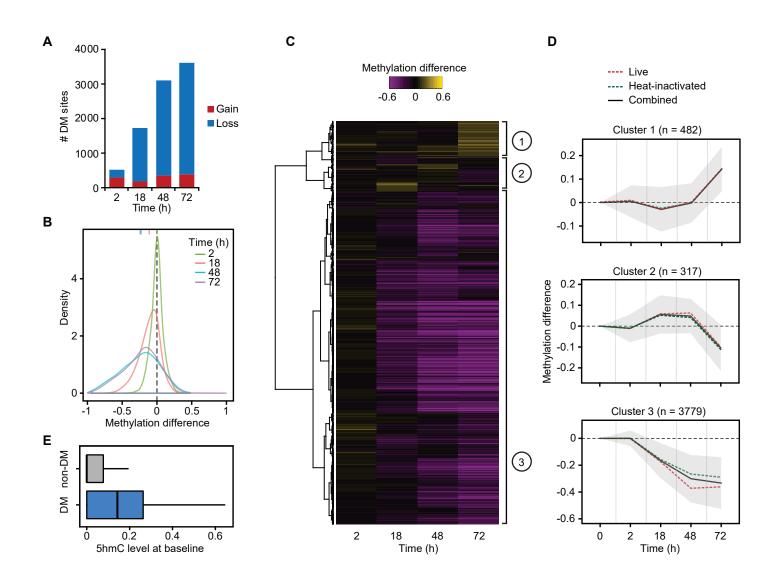
Helin K, Gomez-Vaquero C, Ballestar E: PU.1 target genes undergo Tet2-coupled
demethylation and DNMT3b-mediated methylation in monocyte-to-osteoclast
differentiation. *Genome Biol* 2013, 14:R99.

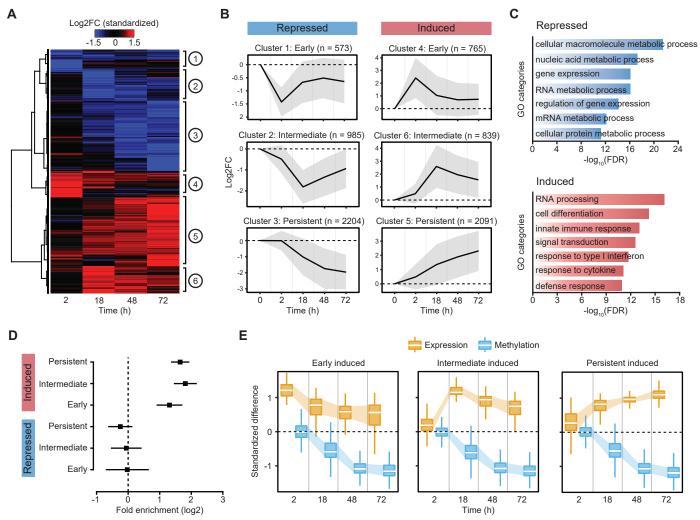
- 41. Rickels R, Herz HM, Sze CC, Cao K, Morgan MA, Collings CK, Gause M, Takahashi YH, Wang
- L, Rendleman EJ, et al: Histone H3K4 monomethylation catalyzed by Trr and mammalian
 COMPASS-like proteins at enhancers is dispensable for development and viability. Nat
 Genet 2017, 49:1647-1653.
- 42. Dorighi KM, Swigut T, Henriques T, Bhanu NV, Scruggs BS, Nady N, Still CD, 2nd, Garcia BA,
 Adelman K, Wysocka J: Mll3 and Mll4 Facilitate Enhancer RNA Synthesis and
 Transcription from Promoters Independently of H3K4 Monomethylation. *Mol Cell* 2017,
 66:568-576 e564.
- 43. Vandenbon A, Kumagai Y, Lin M, Suzuki Y, Nakai K: Waves of chromatin modifications in
 mouse dendritic cells in response to LPS stimulation. *bioRxiv* 2017.

- 44. Quintin J, Cheng SC, van der Meer JW, Netea MG: Innate immune memory: towards a better
 understanding of host defense mechanisms. *Curr Opin Immunol* 2014, 29:1-7.
- 45. Saeed S, Quintin J, Kerstens HH, Rao NA, Aghajanirefah A, Matarese F, Cheng SC, Ratter J,
- Berentsen K, van der Ent MA, et al: Epigenetic programming of monocyte-to-macrophage
- 610 **differentiation and trained innate immunity.** *Science* 2014, **345**:1251086.
- 611 46. Ostuni R, Piccolo V, Barozzi I, Polletti S, Termanini A, Bonifacio S, Curina A, Prosperini E,
- 612 Ghisletti S, Natoli G: Latent enhancers activated by stimulation in differentiated cells. *Cell*613 2013, 152:157-171.
- 47. Kaufmann E, Sanz J, Dunn JL, Khan N, Mendonça LE, Pacis A, Tzelepis F, Pernet E, Dumaine
- 615 A, Grenier J-C, et al: BCG Educates Hematopoietic Stem Cells to Generate Protective Innate
- 616 Immunity against Tuberculosis. Cell 2018, 172:176-190.e119.
- 617 48. Krueger F, Andrews SR: Bismark: a flexible aligner and methylation caller for Bisulfite-Seq
 618 applications. *Bioinformatics* 2011, 27:1571-1572.
- 49. Langmead B, Salzberg SL: Fast gapped-read alignment with Bowtie 2. Nat Methods 2012,
 9:357-359.
- 621 50. Bray NL, Pimentel H, Melsted P, Pachter L: Near-optimal probabilistic RNA-seq
 622 quantification. Nat Biotechnol 2016, 34:525-527.
- 623 51. Anders S, McCarthy DJ, Chen Y, Okoniewski M, Smyth GK, Huber W, Robinson MD: Count-
- based differential expression analysis of RNA sequencing data using R and Bioconductor.
 Nat Protoc 2013, 8:1765-1786.
- 52. Benjamini Y, Hochberg Y: Controlling the False Discovery Rate: A Practical and Powerful
 Approach to Multiple Testing. Journal of the Royal Statistical Society Series B
 (Methodological) 1995, 57:289-300.

629	53.	Bindea G, Mlecnik B, Hackl H, Charoentong P, Tosolini M, Kirilovsky A, Fridman WH, Pages
630		F, Trajanoski Z, Galon J: ClueGO: a Cytoscape plug-in to decipher functionally grouped
631		gene ontology and pathway annotation networks. Bioinformatics 2009, 25:1091-1093.
632	54.	Shen L, Shao N, Liu X, Nestler E: ngs.plot: Quick mining and visualization of next-
633		generation sequencing data by integrating genomic databases. BMC Genomics 2014, 15:284.
634	55.	Li H, Durbin R: Fast and accurate short read alignment with Burrows-Wheeler transform.
635		<i>Bioinformatics</i> 2009, 25: 1754-1760.
636	56.	Khan A, Fornes O, Stigliani A, Gheorghe M, Castro-Mondragon JA, van der Lee R, Bessy A,
637		Cheneby J, Kulkarni SR, Tan G, et al: JASPAR 2018: update of the open-access database of
638		transcription factor binding profiles and its web framework. Nucleic Acids Res 2018,
639		46: D1284.
640	57.	Zhang Y, Liu T, Meyer CA, Eeckhoute J, Johnson DS, Bernstein BE, Nusbaum C, Myers RM,
641		Brown M, Li W, Liu XS: Model-based analysis of ChIP-Seq (MACS). Genome Biol 2008,
642		9: R137.
643	58.	Liao Y, Smyth GK, Shi W: featureCounts: an efficient general purpose program for
644		assigning sequence reads to genomic features. Bioinformatics 2014, 30:923-930.
645		
646		
647		

bioRxiv preprint doi: https://doi.org/10.1101/358531; this version posted June 29, 2018. The copyright holder for this preprint (which was not certified by peer review) is the author/funder, who has granted bioRxiv a license to display the preprint in perpetuity. It is made available under aCC-BY-NC-ND 4.0 International license.





bioRxiv preprint doi: https://doi.org/10.1101/358531; this version posted June 29, 2018. The copyright holder for this preprint (which was not certified by peer review) is the author/funder, who has granted bioRxiv a license to display the preprint in perpetuity. It is made available under aCC-BY-NC-ND 4.0 International license.

